AIP Advances

Investigation for the structural stress of SiO_2 thin films and its distribution on the large-wafer created by plasma enhanced chemical vapor deposition

Cite as: AIP Advances **8**, 085217 (2018); https://doi.org/10.1063/1.5045516
Submitted: 21 June 2018 . Accepted: 14 August 2018 . Published Online: 23 August 2018

DeGui Sun, Qingyu Sun, Wenchao Xing, Zheyu Sun, Hongpeng Shang, Liyuan Chang, Xueping Wang, Peng Liu, and Trevor Hall

ARTICLES YOU MAY BE INTERESTED IN

Capacitive energy harvesting using soft dielectric elastomers: Design, testing and impedance matching optimization
AIP Advances **8**, 085310 (2018); https://doi.org/10.1063/1.5041490

Influences of temperature gradient and distance on the morphologies of MoS_2 domains
AIP Advances **8**, 085218 (2018); https://doi.org/10.1063/1.5050652

Time resolved photoluminescence studies of degradation in GaInP/GaAs/Ge solar cells after 1MeV electron irradiation
AIP Advances **8**, 085213 (2018); https://doi.org/10.1063/1.5034147

Learn more today!

© 2018 Author(s).

AIP ADVANCES **8**, 085217 (2018)

Investigation for the structural stress of SiO_2 thin films and its distribution on the large-wafer created by plasma enhanced chemical vapor deposition

DeGui Sun,[1,2,a] Qingyu Sun,[1] Wenchao Xing,[2] Zheyu Sun,[2] Hongpeng Shang,[1] Liyuan Chang,[1] Xueping Wang,[1] Peng Liu,[3] and Trevor Hall[3]
[1]*School of Science, Changchun University of Science and Technology, 7089 Weixing Road, Changchun, JL 130022, China*
[2]*Jilin Sino-Microelectronics Co. Ltd, 99 Shenzhen Street, Jilin, JL 130031, China*
[3]*Centre for Research in Photonics, University of Ottawa, 25 Templeton Street, Ottawa, ON K1N 6N5, Canada*

(Received 21 June 2018; accepted 14 August 2018; published online 23 August 2018)

For a multilayered configuration of SiO_2 film created by plasma enhanced chemical vapor deposition (PECVD), the thermal stress and growth-caused stress are two intrinsic stresses. In this work, based on the interactions of all the layers of film, a nonlinearly distributed structural stress over a large substrate is found. The numerical simulations for the nonlinear distribution of the structural stress and the uniform distributions of the two intrinsic stresses are carried out. As a result, the tensile structural stress decreases by $\sim 4x10^5$MPa from center to edge of a 6” silicon wafer and the compressive growth-caused stress increases by $\sim 5x10^5$MPa corresponding to the growth-rate increase of 40nm/s, which matches a ~120MPa distribution of residual compressive stress obtained with in-situ measurements of film samples. In simulations, it is also discovered that the initial curvature of substrate has an impressive influence on the later grown film. © *2018 Author(s). All article content, except where otherwise noted, is licensed under a Creative Commons Attribution (CC BY) license (http://creativecommons.org/licenses/by/4.0/).* https://doi.org/10.1063/1.5045516

I. INTRODUCTION

As a mature technical platform, silicon dioxide (SiO_2) waveguide based planar lightwave circuit (PLC) technology is driving the wide adoptions and applications of functional components.[1,2] In research and development of the PLC components, the uniformity and repeatability of refractive index and absorption of a light wave in dielectric thin films are of the important interests.[3–9] In these works, Townsend et al. first performed research on the strain conservation of a multilayered configuration of film and gave a method to modeling stress mechanism;[3] Hsueh started research with the elastic deformation of thin-film to model the asymmetric stress at two orthogonal directions, and then considered the bending caused strains of thin-film;[4] Zhao et al. developed the strain compatibility and the force conservative condition between any two layers in the successive depositions to control the birefringence in optical waveguides;[5] Peralta et al. investigated the depositing conditions of SiO_2 films to compress the birefringence of waveguides;[6] Huang and Yan performed the systematic studies of all possible stresses around waveguide channels;[7] and Heise and Narevich investigated the birefringence on the polarization dependent loss (PDL) of silica-waveguide Mach-Zehnder interferometer (MZI) typed optical switches;[8] Zheng et al. improved the uniformity of SiO_2 waveguides by introducing a silica ridge in a high vacuum gap,[9] and we ever investigated the performance dependences of the silica-waveguide MZI-typed optical switches on the physical parameters determined by manufacturing and then demonstrated a method to controlling the manufacturing quality in our previous work.[10]

[a]sundg@cust.edu.cn

 © Author(s) 2018

We know, when evaluating the maturity of optical waveguide devices and techniques, in addition to the central performance specifications, there is also another factor presenting both the physical property and application potential of PLC components – the stress distribution around waveguides because it plays an important role in reducing the R&D time and yielding a high success-rate, resulting in the broad applications and proliferation of the PLC based optical products in industry.[9,10] So, in this work, the dependence of the structural stress on the position of wafer is taken as a key cutting point for studying the stress distribution of SiO_2 films.

Research on the physical properties of SiO_2 films produced by plasma-enhanced chemical vapor deposition (PECVD) was started around the begin of 1980s, and the some significant achievements have led to the common conclusion that the depositing conditions of machine play a dominant role in determining the stress properties.[11–16] In 1986 Kobeta and Irene first measured the stress distribution of the PECVD-grown SiO_2 films,[11] then in 1991 Windischenmann et al. proposed the flame hydrolysis deposition (FHD) to tailor the over cladding,[12] further in 1996 Carlotti et al. compared the stress properties among the different PECVD depositing conditions,[13] and Chen et al. investigated the thermal process effects on the stress properties.[14] Of the forming mechanisms of film stresses, Hertz first proposed an early contact theory of isotropic elastic spheres of growing dielectric films in 1985 for the case having no frictional interaction.[15] Then, around the begin of this century, Freund and Chason extended this contact theory to the case of elastic solids.[16] In this theory, the deposition of thin film is started with an array of hemispherical grains, then an island having an interaction of two forces to coalesce a thin film, in which the interaction of two forces leads to a stress. In 2012, Chason et al. proposed a kinetic theory to improve their contact theory of the growth-caused stress of films.[17] Then, the tensile stress gradually relaxes and the compressive stress is generated in a triple junction formed by the surface of the last deposited sublayer and the two grain boundaries on this surface.[18,19] In summary, all the above studies are attributed to the two intrinsic stresses that are created during the deposition process and the temperature change process between the inside and outside of vapor chamber, however, these two sources cannot cover all the stresses. So, this work is devoted to investigating another stress source, the structural stress.

In this work, we comprehensively investigate the interactions among multiple layers and substrate to model the structural stress distribution of SiO_2 film over a large substrate in Sec. II. Further, in Sec. III, we carry out the numerical simulations for the distribution of structural stress on the large Si wafer. In Sec. IV, we measure the stress distributions of several SiO_2 thin films deposited on a 6" Si wafer, then discuss the discrepancies between the experimental results and the numerical simulation values in amplitude and further prove a potential of growth-caused stress. Thereby, in Sec. V, we simulate the dependence of growth-caused stress on growth-rate and further analyze the balancing process of these stresses. Finally, in Sec. VI, we give the conclusions.

II. MODELS FOR ALL THE STRESSES OF THIN FILMS

A. Theoretical models for defining the structural stress and its distribution

Figure 1 schematically shows the dual forming processes of structural stress and growth-caused stress of a multilayered SiO_2 film deposited on a thick substrate: Fig. 1(a) is a film shape where the structural stress is caused by the interactions among all the layers and substrate and Fig. 1(b) is a schematic forming process of the growth-caused stress with the film evolution from the isolate grains to a continuous film in a triple junction between two grains and a surface of the last sublayer.

In a multilayered configuration of thin film as shown in Fig. 1, as the growth-caused stress is formed during deposition, the interactions among all the layers and substrate also generate a new stress - the structural stress. Of difference from the growth-caused stress is that the structural stress is mainly dependent on the curvature of multilayered film configuration and related to r, consequently changing the distribution of the final residual stress of the film, while the growth-caused stress depends on the deposition conditions such as the substrate temperature, the gas flow/pressure, and the rf power.

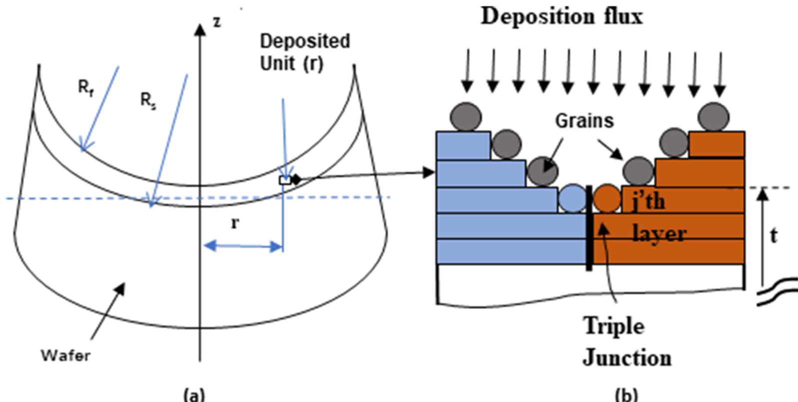

FIG. 1. Schematic forming processes of two stresses in a multilayered film deposited by PECVD and the stresses: (a) the structural stress created by the interactions among all the sublayers and substrate in a film configuration and (b) the growth-caused stress created in the evolution process of a depositing grain, where R_f and R_s, respectively, stand for the surface radii of film and substrate, and t is the thickness of formed film.

In terms of Townsend's theoretical model, we define the structural stress as[3]

$$\sigma_{f,thry} = E_f \cdot [-\ln(d_i) + (\sum_j E_j t_j \ln(d_j)/\sum_j E_j t_j) + (t_n - t)K_f] \tag{1}$$

Where E_f is the elastic modulus of the finished film, E_j is the elastic modulus of the j'th sublayer material, t_j and t are the thickness of the j'th sublayer and the total thickness of the film configuration, respectively.

At the condition of $t_s >> t$, we assume the individual sublayers to be unstrained with relaxed length of d_i after the i'th sublayer is deposited, if v_s and v_i are Poisson ratios of the substrate and the i'th sublayer of film, respectively, the corresponding thickness at this situation is defined as the neutral thickness t_n defined by:

$$t_n = \frac{t_s}{2} + \sum_i \frac{E_i(1-v_s)}{E_s(1-v_i)} \cdot \frac{t_i}{2} \tag{2}$$

In Eq. (2), the curvature K_f should be variable with radius r, so it is theoretically determined by the multilayered configuration with the elastic modulus of each sublayer as

$$K_f = \frac{\sum_i E_i \gamma_i \frac{t_i}{2}[-\ln(d_i) + \sum_j E_j t_j \ln(d_j)/\sum_j E_j t_j]}{\sum_i E_i t_i[(\frac{t_n t}{2} - \frac{t^2}{3}) + (t - t_n)\frac{\gamma_i}{2} - \frac{1}{12}(3\gamma_i^2 + t_i^2 - t^2)]} \tag{3}$$

Where γ_i is a parameter for adjusting the relations between the strain and stress of all sublayers after the i'th sublayer is deposited, which is defined by

$$\gamma_i = \sum_{j=1} \beta_{ij} t_j \tag{4}$$

With the definition as that β_{ij} is -1 for $i > j$, 0 for $i = j$, and 1 for $i < j$. In this model of defining the stress, the elastic modulus is also transferred to the effective modulus by the total widths of the i'th sublayer and bottom layer: w_i and w_0 as

$$E_i^* = E_i/(w_i/w_0) \tag{5}$$

In Eqs. (3) and (4), both d_i and E_i^* are the functions of radius r, so the key parameters t_n and K_f are certainly the functions of r. Therefore, from the definition model Eq. (1) of the structural stress of film, $\sigma_{f,thry}$ is confirmed to be a function of r.

B. Discussions for the two intrinsic stresses

As the first intrinsic stress of films, the thermal stress has a common equation as[20]

$$\sigma_{thm} = \overline{E_f} \cdot \Delta\alpha \cdot \Delta T \tag{6}$$

Where $\Delta\alpha = \alpha_f - \alpha_s$, α_s and α_f are the coefficient of thermal extension (CTEs) of substrate and film, respectively, and ΔT is the temperature difference between the depositing and room conditions. To control the thermal stress of thin films, most of research works are basically focused on two methods: (i) lowering the temperature difference ΔT and (ii) relaxing both the biaxial modulus of film $\overline{E_f}$ and the CTE difference $\Delta\alpha$ with an appropriate annealing process.

As the second intrinsic stress of a thin film, the growth-caused stress has also been attracting much research and typically the prestigious establishment is the kinetic model that combines the contact theory of films and the equilibrium of surface energy in film growing process. In terms of the Chason's kinetic model, after the deposition of the i'th sublayer of film, the growth-caused stress is an effective combination of tensile stress and compressive stress defined by:

$$\sigma_i = \sigma_c + (\sigma_L - \sigma_c)e^{-\delta t/\tau} \tag{7a}$$

With the definitions as

$$\sigma_L = \alpha\left[\frac{\Delta\gamma}{L}\right]^{1/2} \tag{7b}$$

$$\sigma_c = \frac{-\delta\mu_s}{\Omega} \tag{7c}$$

$$\frac{1}{\tau} = \beta \cdot \frac{D}{aL}, \tag{7d}$$

and

$$\beta = \frac{4C_s\overline{E_i}\Omega}{kT} \tag{7e}$$

Where δt is the time interval from the last sublayer to this grain-formed sublayer, $\Delta\gamma$ the energy difference between surface and grain boundary, L the grain size, α a constant depending on the deposition condition, $\delta\mu_s$ the increase in chemical potential of the surface because the film is not in equilibrium during deposition, Ω the volume associated with adding an atom to the grain boundary, D an effective diffusivity related to the rate of hopping from the surface into the triple junction, a the normal size of the atom (same as the sublayer spacing), k the Boltzmann constant, T the absolute temperature, $\overline{E_i}$ the biaxial modulus of the i'th sublayer of film, and C_s a dimensionless concentration (fractional coverage) of mobile atoms on the surface that are free to make diffusive jumps into the triple junction. Finally, the average growth-caused stress of films can be calculated by:

$$\sigma_{grw} \approx \frac{1}{t_f} \cdot \sum_{i}^{N_{layers}} \sigma_i \tag{8}$$

In accordance with our comparing studies of the contact theory and kinetic evolution theory developed by Freund and Chason,[16,17] we set a further understanding as that the growth-caused stress is based on a new conservation of the stress caused forces of each deposited grain, whereas the thermal stress is from a new conservation of the stress caused forces of whole wafer. We know, the deposition parameters used in the set of equations (7a)–(7e), $\Delta\gamma$, L, δt and α are dependent of the depositing conditions: the temperature, mixed ratio of gases, pressure and radio frequency (rf) power, but they are independent of position r. To the contrary, β is dependent on r because the effective elastic modulus E_i^* defined by Eq. (5) is the function of r, and further is τ too. Accordingly, in our simulations, if the structural stress of a film is much lower than the two intrinsic stresses, the effect of the film curvature on E_i^* can be ignorable, otherwise a modulation effect onto the elastic parameters of film needs to be introduced into a new formula as

$$\overline{E_f^*} = E_i^*/(1 - \nu_f) \tag{9}$$

III. NUMERICAL SIMULATIONS

A. Simulations for the structural stress distribution

At the outset a single layer film is set, then for the structural stress defined by Eqs. (1)–(3), the physical parameters related to the elastic stress such as the Young modulus and CTE are not only dependent on the measured position (namely, the distance of measured position from the center, r), but also affected by the other layers and substrate. In accordance with Eq. (3), the starting layer – substrate curvature K_s has an impact upon the final curvature value, so it undoubtedly has an impact upon the structural stress. For a multilayered configuration of films shown in Fig. 1, the 3.0 and 6.0μm thick SiO_2 films are produced by PECVD technique on a 6" diameter wafer having a thickness of 625μm, then by setting three K_s values: 1.0, 10.0 and $100.0m^{-1}$, the dependences of relative curvature K_f/K_s of film on r are numerically simulated as depicted in Figs. 2(a) and 2(b), respectively.

Note from Fig. 2 that when the distance r is from 5mm to 65mm, the K_f/K_s of both either 3.0μm or 6.0μm film almost stays on the constants for the first two K_s values: 1.0 and $10.0m^{-1}$, while it is a nonlinear increase for the K_s value of $100.0m^{-1}$. Thus, we conclude that the curvature of substrate has a paramount important influence on the structural stress distribution, the much lower K_s value is preferred to compress the curvature of film. So, by selecting $K_s = 1.0m^{-1}$, with Eqs. (1)–(3) we carry out the numerical simulations of the structural stress distributions of these two SiO_2 films as shown in Figs. 3(a) and 3(b), respectively, where the horizontal axis means the distance from the measured position to the center of wafer and the vertical axis is the relative curvature K_f/K_s. One

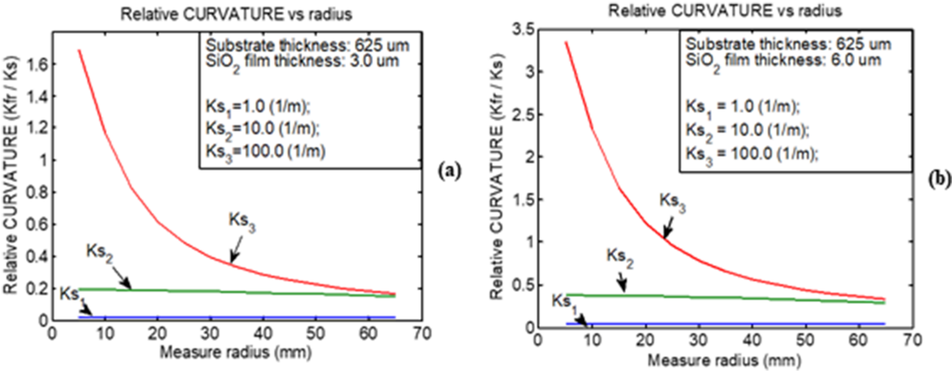

FIG. 2. Numerical simulations for the relative curvature coefficient of SiO_2 film on a 625μm thick Si wafer with respect to three values of substrate curvature, where the film thickness is: (a) 3.0μm and (b) 6.0μm.

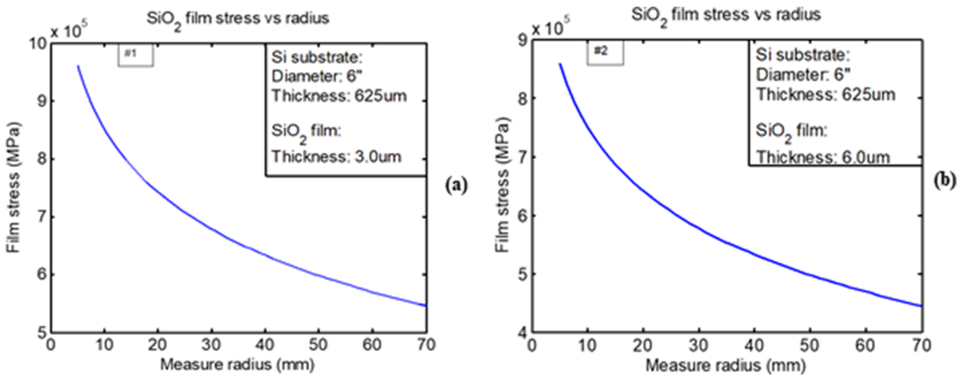

FIG. 3. Numerical simulations for the intrinsic stress of SiO_2 film deposited on a 625μm thick Si wafer where the film thickness is: (a) 3.0μm and (b) 6.0μm.

significant finding from Fig. 3 is that the structural stresses are always positive for these two film thickness values, namely, indicating the tensile stresses that slowly decreases with the film thickness. We also notice from Fig. 3(a) that, for a 3.0μm thick film, the structural stress nonlinearly decreases by $4 \times 10^5 MPa$ when r is from 5mm to 70mm. in contrast to the 3.0μm thick film, for a 6.0μm thick film, the structural stress also nonlinearly increases by $4 \times 10^5 MPa$, too.

In order to comprehensively investigate the dependences of the film structural stress on film thickness and measured position on the wafer, we select a wide range of film thickness: 3-18μm to simulate the structural stress distribution and property of the film with these two parameters, consequently obtain a two-dimensional (2D) distribution of the structural stress as shown in Fig. 4. Note that the structural stress implicitly expresses the distribution trend of the SiO_2 film structural stress that quickly nonlinearly decreases with the measured position r and slowly nonlinearly decreases with the film thickness t.

In terms of the above derivations, simulations and discussions, we can conclude that the structural stress is an extra-stress apart from the two intrinsic stresses: the thermal stress and the growth-caused stress, and finally influences the total residual stress distribution on the whole wafer. In addition, we can notice in Eq. (6) that the CTE difference $\Delta\alpha$ only depends on material, so the thermal stress is independent of the position of substrate, to the contrary, the growth-caused stress defined by Eq. (9) should have a variable distribution on the large substrate.

B. Simulations for the thermal stress and analysis

As analyzed in Sec. II, the interactions among all the sublayers and substrate can cause a nonlinear distribution of structural stress of 3-18μm SiO_2 thin film on a 6" Si wafer, but the absolute stress distribution from the center to the edge of wafer can reach the level of $4 \times 10^5 MPa$, namely, the absolute change of structural stress almost stay at the same level. Compared with the usual values of intrinsic thermal stress, the positive values of structural stress σ_{str} are relatively very high. Then, we numerically calculate the distribution of the new biaxial elastic modulus $\overline{E_f^*}$ of 6μm thick SiO_2 thin film as depicted in Fig. 5. Note that the variation of biaxial elastic modulus caused by the multilayer interactions is too small to take into account, namely, it is only $(\overline{E_f^*}/\overline{E_f} - 1) \approx 0.0013\%$. Thus, in the intrinsic thermal stress calculation, this effect is ignorable.

To study the effect of structural stress on the intrinsic thermal stress of thin films produced by PECVD, it is very necessary to simulate the influences of the new $\overline{E_f^*}$ on the thermal stress. In Eq. (6), for $\Delta\alpha = \alpha_f - \alpha_s$, a typical value is around 2.9×10^{-6} (1/K) and ΔT that is used for depositing the films

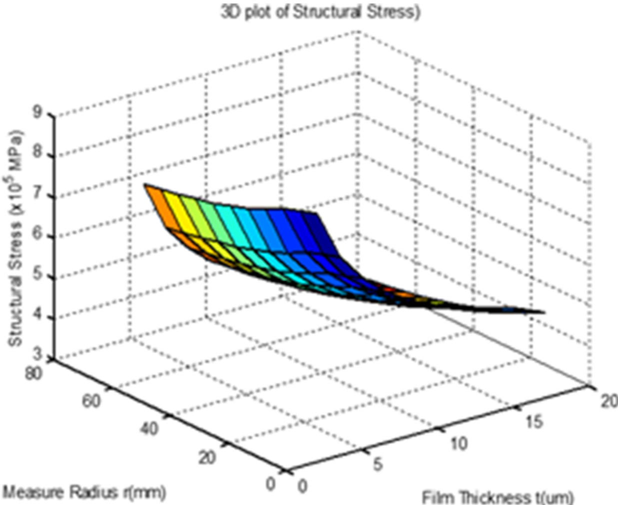

FIG. 4. Numerical simulation result of the dependence of SiO_2 film structural stress on both the measured position on wafer and the film thickness, where the curvature of substrate K_s is selected to be 1.0 m^{-1}.

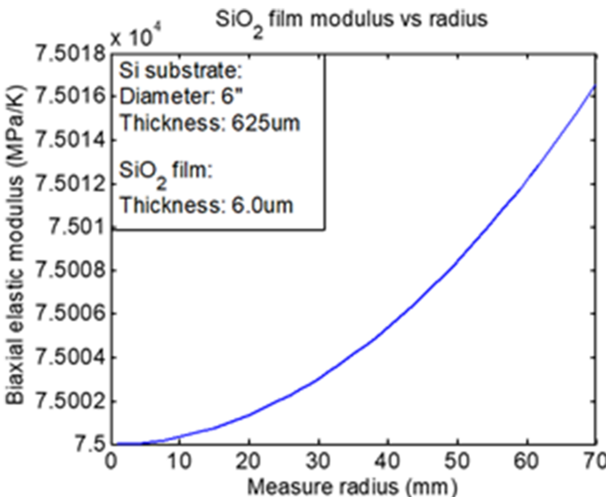

FIG. 5. Numerical simulation for the biaxial elastic modulus variation of SiO_2 film, where the insets indicate the dimension of Si substrate and the thickness of SiO_2 film.

is around 400°C, then we obtain the numerical results for the $\Delta\alpha$ range from $-4.0 \times 10^{-6}K^{-1}$ to $-2.0 \times 10^{-6}K^{-1}$ as shown in Fig. 6. Note that the amplitude of intrinsic thermal stress is not only uniformly distributed on a large Si wafer, but its amplitude is much lower than the corresponding numerical simulation results shown in Fig. 3. In addition, the theoretical model for defining the thermal stress of thin films Eq. (6) does not include the thickness of film, which immediately gives rise to a conclusion as that this thermal stress model is based on an average stress value of the film. For the illustrative case, at the condition of $\Delta\alpha = 4.0 \times 10^{-6}(1/K)$ and $\Delta T = 400^oC$ in Fig. 6, the thermal stress value is only -120MPa. However, the structural stress is an extra-stress imposed on the sum of two intrinsic stresses: the growth-caused stress and the thermal stress. Finally, the sum of three stresses leads to the steady state stress σ_{ss}.

By investigating the values and properties of some physical and chemical parameters that are used in the set of equations from (7a) to (7e), we find that the growth-caused stress has its very complex dependences on the growth process and parameters. As mentioned above, the curvature effect of the whole film has little effect on the biaxial elastic modulus $\overline{E_f}$ of film, so σ_{thm} does not depend on the

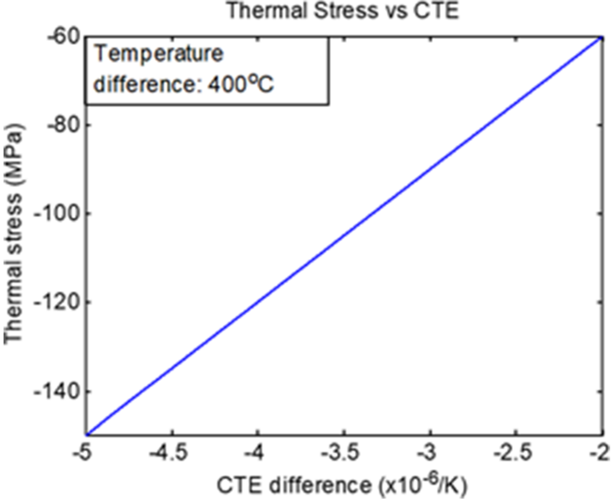

FIG. 6. Numerical simulations for the thermal stress of SiO_2 film versus the thermal extension coefficient difference where temperature difference is set as 400°C.

r of wafer.[17,21,22] The growth-caused stress σ_{grw} and the structural stress σ_{str} are intimately linked during the deposition, then the resulting residual stress further determines the central parameter α_f of the thermal stress σ_{thm}. During the deposition of the i'th sublayer of film, its σ_{grw} is best fitting to a kinetic competition model of different mechanism that not only depends on the growth rate, the diffusivity and the grain size, but it is also related to the absolute temperature T, then produces the direct effects on such the central physical parameters of the deposited film as E_f and α_f, which further affect σ_{str} with the curvature K_f and σ_{thm} with the variations of both E_f and α_f. Consequently, the final steady state stress σ_{ss} (i.e., the residual stress of film) is the algebraic sum of these three stresses as

$$\sigma_{ss} = \sigma_{str} + \sigma_{thm} + \sigma_{grw} \tag{10}$$

All the above numerical simulations are performed by the Matlab Programs.

IV. EXPERIMENTAL MEASUREMENTS AND DISCUSSION

The nine points for stress distribution measurements are schematically shown in Fig. 7. In fact, as labeled with dashed line in Fig. 7, the nine points stand for nine circles having different radii with an equal adjacent radius difference of 15mm from the center to the edge of wafer, namely, point 5 is at the center, points 4 and 6 are at the radius of 15mm, points 3 and 7 at 30mm, points 2 and 8 at 45mm, and points 1 and 9 at 60mm, the significant outside circle. Then we measure the birefringence values on the nine selected positions on wafer by using the Metricon 2010 Prism Coupler and further calculate the stress distribution with the theoretical model relating to the birefringence and the stress of film.[23] As a practical work, at the depositing temperature of 400°C we create three samples of 6µm thick SiO_2 thin films with respect to three different SiH_4 flux values: 217, 250 and 265sccm and then create the other two samples of 3µm thick SiO_2 thin films with respect to two different BPSG fluxes.

At the wavelength of 1539nm we measure the birefringence values of all the samples of SiO_2 thin films first, and then obtain the corresponding residual stress values of three 6µm thick SiO_2 films and two 3µm thick SiO_2 films as shown in Figs. 8(a) and 8(b), respectively. Note from Fig. 8(a) that all the stress values are minus, which stand for the compressive stresses of SiO_2 films, in which one SiH_4 flux value, 217sccm, obviously shows a compressive stress increase of more than 120MPa from the center to edge of wafer. When the SiH_4 flux increase to 250sccm, this variation gradually becomes weak, but the amplitude of the compressive stress is uniformly higher than the case of 217sccm. Note from Fig. 8(b) that two different BPSG fluxes have the same compressive stress increases of more than 120MPa from the center to the edge of wafer. Thereby, it is concluded from Fig. 8 that a trend of the final stress distribution from the center to the edge of wafer can reach more than 120MPa.

Obviously, the experimental results of compressive stress shown in Fig. 8 are too far from the equilibrium with the algebraic sum of the numerical simulation values of the structural stress shown

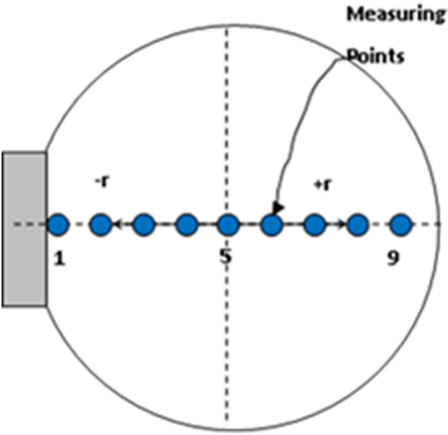

FIG. 7. Measurements for the stress distribution of a silicon dioxide film on 6″ Si wafer with a prism coupler - Metricon-2010.

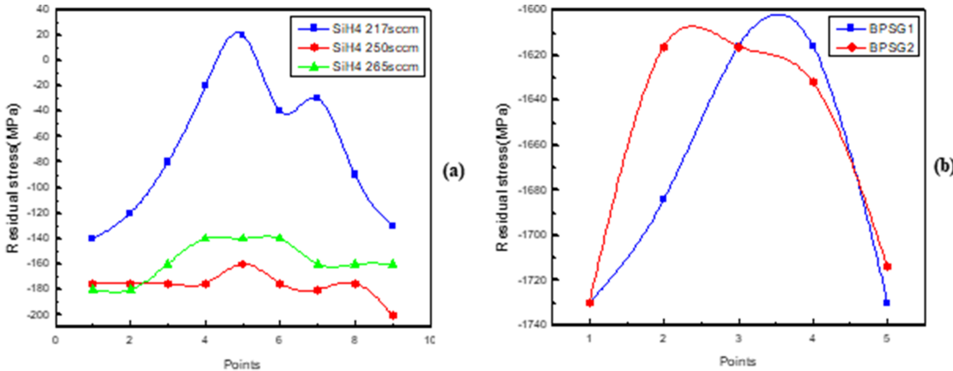

FIG. 8. Measurements for the stress distributions of SiO_2 films on a 6" wafer Metricon-2010 prism coupler at$\lambda = 1539nm$: (a) for the 6.0μm thick film with respect to three flux values of SiH4 and (b) for the 3.0μm thick film with respect to two flux values of BPSG.

in Fig. 3 and the thermal stress shown in Fig. 6. In terms of the obvious differences between the experimental results and the numerical calculation results of ($\sigma_{str} + \sigma_{thm}$), we can conclude, as predicted above, σ_{grw} of SiO_2 films is not only the compressive stress at the order of $10^5 MPa$, but it also has the similar distribution with σ_{str} under the same deposition conditions.

V. ANALYSIS FOR THE DIFFERENCES BETWEEN THE NUMERICAL VALUES AND EXPERIMENTAL RESULTS

As mentioned above, the numerical simulations show that, when r is from 5mm to 70mm, the structural stress has the changes of about $4 \times 10^5 MPa$ for both the 3.0 and 6.0μm SiO_2 films, the thermal stress is at the level of $-120MPa$ and uniformly distributes on wafer, while the measured stress variance from the center to the edge of wafer is only about $-100MPa$. Consequently, it is concluded that only the growth-caused stress can form such big stress differences. With Eqs. (7a)–(7e) we obtain the simulation results of the growth-rate dependence of growth-caused stress with respect to three normalized atom sizes: 0.25, 0.50 and 0.75μm as shown in Fig. 9. Note that the growth-caused stress is $-8.0 \times 10^5 \sim -2.0\times10^5 MPa$ when the growth rate is from 10nm/s to 50nm/s, which can exactly balance the numerical values of the structural stress, leading to a conclusion that at the lower growth rate (e.g. <20nm/s), the lower the normalized size of atoms leads to the higher compressive

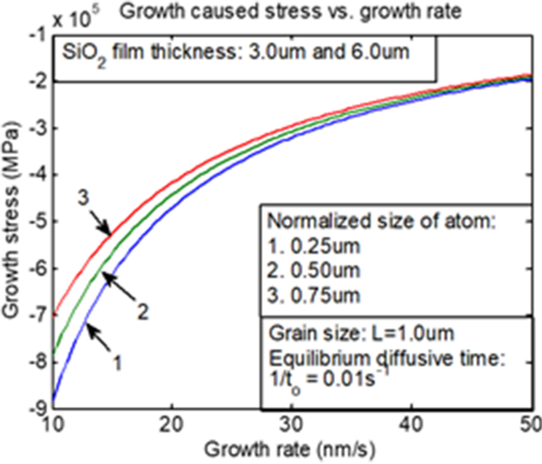

FIG. 9. Numerical simulations for the growth-caused stress of SiO_2 film vs the growth-rate, where the parameters used in simulations are set as: $L = 1.0\mu m$, $\beta D = 0.117 \times 10^{-15} m^2/s$, $\Delta\gamma = 0.13J$, $\delta\mu_s = 0.13 \times 10^{-6}V$, and $1/\tau = 0.01s^{-1}$.

growth-caused stress. Accordingly, of the parameters $\Delta\gamma$, L, α, $\delta\mu_s$ and D, some can be used to manipulate the distribution of σ_{grw}.

VI. CONCLUSIONS

The conclusions in this work are that the nonlinear distribution of a structural stress over the wafer and the unbalance of the algebraic sum of the structural stress and the thermal stress with the experimental measurements of the final residual stress gives a convincible way to estimating the growth-caused stress.

ACKNOWLEDGMENTS

This work is co-sponsored by the R&D/Education Fund Society of Changchun University of Science and Technology (CUST), China, the Natural Science Foundation of Jilin Province Science and Technology Department (20180101223JC) and (20160101263JC), the In-Kind invest of Jilin Sino-Microelectronics Corporation, Jilin, China, and the In-Kind Invest of D&T Photonics (DTP), a spun-off startup from University of Ottawa, Canada, the 321 Grant of Nanjing Government, and the Fundamental/in-kind invests of Jilin Sino-Microelectronics Co. Ltd.

[1] C. R. Doerr and K. Okamoto, *Optical Fiber Telecommunications V* (Academic Press, New York, 2008).
[2] S. N. Takoto, K. Jinguiji, M. Yasu, H. Toba, and M. Kawachi, IEEE/OSA J. Lightw. Technol. **6**, 1003–1010 (1988).
[3] P. Townsend, D. Barnett, and T. Brunner, J. Appl. Phys. **62**, 4438–4444 (1987).
[4] C.-H. Hsueh, J. Appl. Phys. **91**, 4438–4444 (2002).
[5] X. L. Zhao, Y. Z. Xu, and C. Li, IEEE/OSA J. Lightw. Technol. **21**, 2352–2357 (2003).
[6] L. G. de Peralta, A. A. Bernussi, H. Temkin, M. M. Borhani, and D. E. Doucette, IEEE J. Quantum. Electron. **39**, 874–879 (2003).
[7] M. Huang and X. Yan, J. Appl. Phys. **95**, 2820–2826 (2004).
[8] G. Heise and R. Narevich, IEEE Photon. Technol. Lett. **17**(10), 2116–2118 (2005).
[9] D. W. Zheng, J. Fong, Z. Shao, L. Liang, and C. Wu, Opt. Exp. **34**, 1753–1758 (2004).
[10] J. Wang, J. Yi, L. Guo, P. Liu, T. J. Hall, and D. G. Sun, Opt. Las. Technol. **89**, 208–213 (2017).
[11] M. Huang, IEEE J. Quantum. Electron. **40**, 1562–1568 (2004).
[12] E. Kobeta and E. A. Irene, J. Vac. Science & Technol. B **4**, 720–722 (1986).
[13] H. Windischenmann, J. Vac. Science & Technol. A **9**, 2459–2463 (1991).
[14] G. Carlotti, L. Doucet, and M. Dupeux, J. Vac. Science & Technol. B **14**, 3460–3464 (1996).
[15] K. L. Johnson, *Contact Mechanics* (Cambridge University Press, Cambridge, UK, 1985).
[16] L. B. Freund and E. Chason, J. Appl. Phys. **89**, 4866–4873 (2001).
[17] E. Chason, J. W. Shin, S. J. Hearne, and L. B. Freund, J. Appl. Phys. **111**, 083520 (2012).
[18] E. Chason and A. M. Engwall, J. Thin Sol. Films **596**, 2–7 (2015).
[19] E. Chason, M. Karlson, J. J. Colin, D. Magnfalt, K. Sarakinos, and G. Abadias, J. Appl. Phys. **119**, 145307 (2016).
[20] G. Guan, A. R. Bruccoleri, R. K. Heilmann, and M. L. Schattenburg, J. Micromech. & Microeng. **24**, 027001 (2014).
[21] Y. Zheng, B. Tao, and Z. Yin, J. Crys. Grow. **405**, 73–80 (2014).
[22] E. Chason, B. W. Sheldon, L. B. Freund, J. A. Floro, and S. J. Hearne, Phys. Rev. Lett. **88**, 156103 (2014).
[23] W. N. Ye, D.-X. Xu, S. Janz, P. Cheben, M.-J. Picard, B. Lamontagne, and N. G. Tarr, J. Lightwave Technol. **23**, 1308–1318 (2005).